Available online at www.sciencedirect.com
ScienceDirect
International Journal of Solids and Structures 44 (2007) 3756–3772
INTERNATIONAL JOURNAL OF SOLIDS and STRUCTURES
www.elsevier.com/locate/ijsolstr

Application of results on Eshelby tensor to the determination of effective poroelastic properties of anisotropic rocks-like composites

A. Giraud [a,b,*], Q.V. Huynh [b], D. Hoxha [b], D. Kondo [c]

[a] LPMM-UMR CNRS 7554/ISGMP, Université Paul Verlaine-Metz, Ile du Saulcy, 57045, Metz Cedex 01, France
[b] LAEGO-ENSG,BP40, Vandoeuvre-lès-Nancy Cedex, F-54501 France
[c] LML-UMR CNRS 8107, USTL, cité scientifique, boulevard Paul-Langevin, 59655 Villeneuve d' Ascq Cedex, France

Received 6 March 2006; received in revised form 31 August 2006; accepted 16 October 2006
Available online 21 October 2006

Abstract

The present work is devoted to the determination of the macroscopic poroelastic properties of anisotropic elastic porous materials saturated by a fluid under pressure. It makes use of the theoretical results provided by Withers [Withers, P.J., 1989. The determination of the elastic field of an ellipsoidal inclusion in a transversely isotropic medium, and its relevance to composite materials. Philosophical Magazine A 59 (4), 759–781.] for the problem of an ellipsoidal inclusion embedded in a transversely isotropic elastic medium. The particular case of a spherical inclusion is very important for rock-like composites such as argillite and shales. The implementation of these results in a micromechanical theory of poroelasticity allows to quantify the effects of the solid matrix anisotropy and of pore space on the effective poromechanical properties. Closed form expressions of Biot tensor and of Biot modulus are presented as well as numerical applications for anisotropic shales.

Keywords: Eshelby tensor; Transverse isotropy; Spherical inclusion; Micromechanics; Biot tensor; Poroelasticity

1. Introduction

This paper treats the estimation of the effective poroelastic properties of rock like composites by using the Eshelby and Hill polarization tensors for an ellipsoidal inhomogeneity in a transversely isotropic elastic material. As the particular case of the spherical inhomogeneity is very important for practical applications, it will be detailed in this paper. This problem is a particular case of the problem of the ellipsoidal inclusion in a transversely isotropic elastic material treated by Withers (1989). A general solution of this problem has been recently presented by Sevostianov et al. (2005) for various inhomogeneities (including spherical inhomogeneity) in a transversely isotropic material. Kirilyuk and Levchuk (2005) present a solution based on Fourier transform

* Corresponding author.
E-mail address: Albert.Giraud@univ-metz.fr (A. Giraud).

0020-7683/$ - see front matter © 2006 Elsevier Ltd. All rights reserved.
doi:10.1016/j.ijsolstr.2006.10.019

method for the same problem. Suvorov and Dvorak (2002) presented solutions for Hill polarization tensor $\mathbb{P}$ of ellipsoidal inclusions in an anisotropic medium, including the particular case of the spheroidal inclusion in a transversely isotropic solids, with a numerical method for integration of the solution (Gaussian integration rule). Analogous solutions for Eshelby tensor in anisotropic solids have been presented recently for piezoelectric materials (see Dunn and Wienecke (1997), Mikata (2000, 2001). Withers' method has been applied in this paper in the particular case of the spherical inhomogeneity. The interest of this method, which is a natural extension of the classical Eshelby's method in the isotropic case (see Eshelby (1957, 1961)), is that it is based upon the analytical integration of the exact Green's function obtained by Pan and Chou (1976) for the transversely isotropic material. It must be emphasized that the Withers' solution deduced in the particular case of the spherical inclusion in a transversely isotropic medium can be useful for sedimentary rocks such as shales. For this class of materials which can be constituted by a transversely isotropic argillaceous matrix with spherical inclusions of quartz and carbonates, we obtain results for the effective poroelastic properties (Biot tensor, Biot modulus). In particular the respective influence of the *matrix* (or *solid particle*) anisotropy and of the pore space morphology on the effective anisotropy of the porous medium at the macroscopic scale are evaluated. The results are compared with elastic moduli characterized by laboratory experiment.

2. Hill polarization tensor for the ellipsoidal inclusion in a transversely isotropic solid

We consider an unbounded domain of an infinite three-dimensional transversely isotropic medium with stiffness $\mathbb{C}$ containing an ellipsoidal inhomogeneity Ω having elastic properties different from those of the surrounding material. In this paper, we generally deal with oblate or prolate spheroidal inhomogeneities whose half-lengths (centered at the origin O) are denoted respectively a in the plane $z_1 - z_2$ and $c = a\varepsilon$ (the symmetry axis is z_3); ε defines the aspect ratio of the ellipsoïd. Consequently, an ellipsoïdal inhomogenity aligned in the principal directions of the rectangular cartesian coordinate system (z_1, z_2, z_3) is geometrically characterized by

$$\underline{z} \in \Omega \Longleftrightarrow \frac{z_1^2 + z_2^2}{a^2} + \frac{z_3^2}{a^2\varepsilon^2} \leqslant 1 \tag{1}$$

The fourth order Hill polarization tensor $\mathbb{P}$ of the ellipsoidal inhomogeneity can be obtained from the second order derivatives of Green's function $\boldsymbol{G}(\underline{z} - \underline{z}')$ (see among others Mura (1987), Nemat-Nasser and Hori (1993))

$$P^{\Omega}_{ijkl}(\underline{z}) = \frac{1}{4}\left(\mathscr{M}^{\Omega}_{kijl}(\underline{z}) + \mathscr{M}^{\Omega}_{kjil}(\underline{z}) + \mathscr{M}^{\Omega}_{ljik}(\underline{z}) + \mathscr{M}^{\Omega}_{ljki}(\underline{z})\right), \quad \underline{z} \in \Omega \tag{2}$$

$$\mathscr{M}^{\Omega}_{ijkl}(\underline{z}) = -\int_{\Omega} G_{ij,kl}(\underline{z} - \underline{z}')\mathrm{d}\Omega_{z'} = -\frac{\partial}{\partial z_l}\int_{\Omega} \frac{\partial G_{ij}(\underline{z} - \underline{z}')}{\partial z_k}\mathrm{d}\Omega_{z'} \tag{3}$$

The Green's function G_{ij}, has been provided by Pan and Chou (1976) for the transversely isotropic material. The reader can find in the reference Withers (1989) the analytical expressions of the Eshelby tensor $\mathbb{S}^{\mathrm{E}}$ for this problem. The corresponding components of Hill polarization tensor can be easily deduced by using the relations (see Appendix A for explicit formula for transversely isotropic medium)

$$S^{\mathrm{E}\Omega}_{ijmn} = P^{\Omega}_{ijpq}C_{pqmn} \tag{4}$$

The components of Hill polarization tensor can be expressed as

$$\begin{aligned} &P^{\Omega}_{1111} = P^{\Omega}_{2222} = P_{11}, \quad P^{\Omega}_{1122} = P^{\Omega}_{2211} = P_{12}, \quad P^{\Omega}_{1133} = P^{\Omega}_{3311} = P_{13} \\ &P^{\Omega}_{3333} = P_{33}, \quad P^{\Omega}_{1313} = P^{\Omega}_{2323} = P_{44}, \quad P^{\Omega}_{1212} = \frac{P^{\Omega}_{1111} - P^{\Omega}_{1122}}{2} \end{aligned} \tag{5}$$

As the particular case of the spherical inhomogeneity ($\varepsilon = 1$ in relation 1) is very important for many practical applications, compact expressions of the Hill polarization tensor obtained by following the Withers' method are recalled in Appendix B. In the particular case of a spherical inclusion in an isotropic medium

$$\mathbb{C} = 2\mu\mathbb{K} + 3k\mathbb{J}, \quad \mathbb{S} = \frac{\mathbb{K}}{2\mu} + \frac{\mathbb{J}}{3k}$$
$$I_{ijkl} = \frac{1}{2}(\delta_{ik}\delta_{jl} + \delta_{il}\delta_{jk}), \quad J_{ijkl} = \frac{1}{3}(\delta_{ij}\delta_{kl}), \quad K_{ijkl} = I_{ijkl} - J_{ijkl}$$
$$k = \frac{E}{3(1-2\nu)}, \quad \mu = \frac{E}{2(1+\nu)} \tag{6}$$

the Eshelby tensor $\mathbb{S}^{E}$ and Hill polarization $\mathbb{P}$ tensor are given by

$$\mathbb{P} = \frac{\alpha}{3k}\mathbb{J} + \frac{\beta}{2\mu}\mathbb{K}, \quad \mathbb{S}^{E} = \mathbb{P} : \mathbb{C} = \alpha\mathbb{J} + \beta\mathbb{K}$$
$$\alpha = \frac{3k}{3k+4\mu} = \frac{1+\nu}{3(1-\nu)}, \quad \beta = \frac{6(k+2\mu)}{5(3k+4\mu)} = \frac{2(4-5\nu)}{15(1-\nu)} \tag{7}$$

3. Determination of poromechanical properties

In this section applications of the solution for the spherical inclusion in a transversely isotropic medium to determine effective properties of porous materials such as shales or argillite are presented. Ulm et al. (2005) used spherical inclusions to represent inclusions of mineral such as quartz or carbonate embedded in a transversely isotropic porous argillaceous matrix for shale type materials. Levin and Markov (2005) used the solution for a spheroidal inhomogeneity to determine the effective elastic moduli and velocities of elastic wave propagation in transversely isotropic solid containing aligned spheroidal inhomogeneities. Recently, Lutz and Zimmerman (2005) investigated the effect of spherical inclusions on bulk modulus and thermal conductivity in the isotropic case. The objective of this section is to study the separate influence of *initial* anisotropy of the matrix and of the anisotropy of the porous space on the effective poroelastic properties such as Biot tensor. Comparisons to experimental results obtained for a clayey material are presented.

3.1. Biot tensor in a transversely isotropic medium

We briefly recall in this section Biot's linear poroelasticity constitutive equations and compatibility relations between the skeleton properties and the matrix properties m (see Coussy (2004), Coussy et al. (1998), Dormieux et al. (2006)). The isothermal linear poroelastic behaviour at the macroscopic scale writes

$$\boldsymbol{\Sigma} = \mathbb{C}^{\hom} : \boldsymbol{E} - \boldsymbol{B}P$$
$$\phi - \phi_0 = \boldsymbol{B} : \boldsymbol{E} + \frac{P}{N} \tag{8}$$

$\mathbb{C}^{\hom}, \boldsymbol{B}, N$, respectively represent the fourth order drained stiffness tensor of the skeleton, the second order Biot tensor and the solid Biot modulus (Dormieux et al. (2006) p. 141). $\boldsymbol{\Sigma}, \boldsymbol{E}, P, \phi, \phi_0$, respectively represent the second order macroscopic stress and strain tensors, the pore pressure, the lagrangian porosity (ratio between volume of pore space and initial volume of porous medium) in the current and reference configuration. The reference configuration is defined by $\boldsymbol{E} = 0$ and $P = 0$. The macroscopic Biot tensor $\boldsymbol{B}$ can be expressed as function of drained macroscopic elastic tensor $\mathbb{C}^{\hom}$ of the skeleton and of the elastic compliance tensor $\mathbb{S}_m$ of the solid matrix m (see Dormieux et al. (2002) and Dormieux (2005))

$$\boldsymbol{B} = \boldsymbol{\delta} : (\mathbb{I} - \mathbb{S}_m : \mathbb{C}^{\hom}), \quad B_{ij} = \delta_{kl}(I_{lkij} - S^{m}_{lkmn}C^{\hom}_{nmij}) \tag{9}$$
$$\frac{1}{N} = (\boldsymbol{B} - \phi_0\boldsymbol{\delta}) : \mathbb{S}_m : \boldsymbol{\delta} = (B_{ij} - \phi_0\delta_{ij})S^{m}_{jikl}\delta_{lk} \tag{10}$$
$$\boldsymbol{\delta} = \delta_{kl}\underline{e}_k \otimes \underline{e}_l, \quad \delta_{kl} = 1 \quad \text{if} \quad k = l, \quad \delta_{kl} = 0 \quad \text{if} \quad k \neq l \tag{11}$$

As an example, relation (9) will be expanded in three particular cases:

- (i) transversely isotropic skeleton ($\mathbb{C}^{\hom}$) and matrix ($\mathbb{C}_m$ and $\mathbb{S}_m$) with the same axis of revolution O_{x_3} (effective transverse isotropy is due to the matrix and the aligned pores),
- (ii) transversely isotropic skeleton with axis of revolution O_{x_3} and isotropic matrix (with bulk modulus k_m, the effective transverse isotropy is only due to the aligned pores),
- (iii) isotropic skeleton (with bulk modulus $k^{\hom}$) and isotropic matrix

In case (i), the macroscopic Biot tensor can be explicitely written in terms of four moduli elastic of the solid matrix and the corresponding moduli of the drained stiffness tensor of the skeleton: E_1^m, E_3^m, ν_{12}^m, ν_{31}^m and $E_1^{\hom}$, $E_3^{\hom}$, $\nu_{12}^{\hom}$, $\nu_{13}^{\hom}$

$$
\begin{aligned}
&\boldsymbol{B} = b_1(\underline{e}_1 \otimes \underline{e}_1 + \underline{e}_2 \otimes \underline{e}_2) + b_3 \underline{e}_3 \otimes \underline{e}_3,\\
&b_1 = 1 + \frac{\frac{1-\nu_{12}^m}{E_1^m} + \frac{\nu_{31}^{\hom}(1-2\nu_{31}^m)-\nu_{31}^m}{E_3^m}}{\frac{2(\nu_{31}^{\hom})^2}{E_3^{\hom}} - \frac{1-\nu_{12}^{\hom}}{E_1^{\hom}}},\\
&b_3 = 1 + \frac{E_3^{\hom}\frac{1-\nu_{12}^{\hom}}{E_1^{\hom}}\frac{1-2\nu_{31}^m}{E_3^m} - 2\nu_{31}^{\hom}\left(\frac{\nu_{31}^m}{E_3^m} - \frac{1-\nu_{12}^m}{E_1^m}\right)}{\frac{2(\nu_{31}^{\hom})^2}{E_3^{\hom}} - \frac{1-\nu_{12}^{\hom}}{E_1^{\hom}}},\\
&\frac{1}{N} = 2(b_1-\phi_0)\left(\frac{1-\nu_{12}^m}{E_1^m} - \frac{\nu_{31}^m}{E_3^m}\right) + (b_3-\phi_0)\left(\frac{1-2\nu_{12}^m}{E_1^m}\right)
\end{aligned}
\tag{12}
$$

In case (ii) it reduces to

$$
b_1 = 1 + \frac{1+\nu_{31}^{\hom}}{3k_m\left(\frac{2(\nu_{31}^{\hom})^2}{E_3} - \frac{1-\nu_{12}^{\hom}}{E_1^{\hom}}\right)} \tag{13}
$$

$$
b_3 = 1 + \frac{E_3^{\hom}\left(\frac{2\nu_{31}^{\hom}}{E_3^{\hom}} + \frac{1-\nu_{12}^{\hom}}{E_1^{\hom}}\right)}{3k_m\left(\frac{2(\nu_{31}^{\hom})^2}{E_3^{\hom}} - \frac{1-\nu_{12}^{\hom}}{E_1^{\hom}}\right)} \tag{14}
$$

$$
\frac{1}{N} = \frac{2b_1 + b_3 - 3\phi_0}{3k_m}
$$

and in case (iii) to the well known relation (see reference book Coussy (2004))

$$
b_1 = b_3 = b = 1 - \frac{k^{\hom}}{k_m}, \quad \frac{1}{N} = \frac{b-\phi_0}{k_m} \tag{16}
$$

$$
E_i^{\hom} = E^{\hom}, \quad \nu_{ij}^{\hom} = \nu^{\hom}, \quad k^{\hom} = \frac{E^{\hom}}{3(1-2\nu^{\hom})} \tag{17}
$$

The objective of next section is to study the separate effects of anisotropy of the matrix and of the anisotropy of the pore space on the macroscopic effective properties: Biot tensor and drained stiffness tensor. The anisotropy of the porous skeleton depends both on the matrix anisotropy and on pore space morphology: pore shape and pore distribution. Relations (12, 13) indicate that Biot tensor is not hydrostatic in cases (i) and (ii) which correspond to a transversely isotropic macroscopic elastic behaviour. In case (i) the deviatoric part of Biot tensor can be attributed to matrix anisotropy and to skeleton anisotropy (including pore space morphology) whereas in case (ii) the deviatoric part is only due to the pore space morphology.

3.2. Homogenization schemes and effective properties

Micromechanical approach aims at determining the macroscopic behaviour of heterogeneous materials from the solution of a boundary value problem defined on the representative volume element (RVE) at the microscopic scale (see Zaoui (1997); Torquato (2002); Dormieux et al. (2006, 2002)). In this paper, we consider

a RVE of a porous solid material occupying the geometrical domain Ω with boundary $\partial\Omega$. Two phases have to be distinguished: the solid particle or *matrix* occupies a domain Ω_m and the porosity occupies the domain Ω_p

$$\Omega = \Omega_p \cup \Omega_m, \quad \Omega_p = f_p\Omega, \quad \Omega_m = (1 - f_p)\Omega \tag{18}$$

The pore space Ω_p is assumed to be made of a set of pores that can be described as inclusions of similar ellipsoidal shape (see Dormieux (2005)). We consider in this paper porous media saturated with water (fully saturated case). An extensive bibliography on homogenization methods can be found in Zheng and Du (2001) for the general case of composites of the matrix-inclusion type, in Levin and Markov (2005) for the particular case of transversely isotropic rocks and in Xu (1998) and Jakobsen and Johansen (2005) for anisotropic rocks. Many authors used the self-consistent scheme. For low and *moderate* porosity, approximately ($f_p \leqslant 0.20$), and for materials such as deep clayey formations, the Mori–Tanaka homogenization scheme provides correct results for elastic and poroelastic properties (see Ulm et al. (2005), Giraud et al. (2005)). It may be noticed that in the case of orientational distribution of non-spherical inclusions, the Ponte Castañeda - Willis scheme (Ponte Castañeda and Willis (1995)) can be used instead of Mori–Tanaka scheme (see Jakobsen and Johansen (2005) for applications of this estimate to porous rocks). In this paper, two particular and simple cases are investigated, the *fully drained* case obtained with $P = 0$ in relations (8), and the *fully undrained* case which can be deduced from poroelastic relations by assuming zero fluid mass supply. The *fully undrained* case presented in this paper is valid only if uniform initial stress and initial pore pressure are equal to zero (zero stress, pore pressure and effective stress). Under a mechanical loading, the undrained poroelastic material behaves simply as a two-phase elastic material, one is the solid matrix, and one is the liquid water which is modelled as an isotropic elastic material with zero shear coefficient ($\mu_p = 0$)

$$\mathbb{C}_p = 3k_p\mathbb{J}, \quad k_p = k_{lq} \approx 2000 \text{ MPa} \tag{19}$$

In the drained case, the stiffness tensor of the pore fluid phase is assumed to be equal to zero. The first case (*fully drained*) gives the drained elastic stiffness tensor $\mathbb{C}^{\text{hom}}$ and the second case (*fully undrained*) gives the undrained elastic stiffness tensor which depends on mechanical properties of the pore fluid phase and of the solid matrix. It may be noticed that (unfortunately) drained experiments are very difficult to perform on very low permeable geomaterials such as shales, argillites or claystones. In many cases, only undrained stiffness coefficients can be evaluated thanks to short term mechanical tests. The drained and undrained effective stiffness tensor corresponding to Mori–Tanaka homogenization scheme can be written as

$$\mathbb{C}^{\text{MT}}_{\text{dr}} = (1 - f_p)\mathbb{C}_m : [(1 - f_p)\mathbb{I} + f_p[\mathbb{I} - \mathbb{P}_m : \mathbb{C}_m]^{-1}]^{-1} \tag{20}$$

$$\mathbb{C}^{\text{MT}}_{\text{undr}} = \mathbb{C}_p - (1 - f_p)(\mathbb{C}_p - \mathbb{C}_m) : [(1 - f_p)\mathbb{I} + f_p[\mathbb{I} + \mathbb{P}_m : (\mathbb{C}_p - \mathbb{C}_m)]^{-1}]^{-1} \tag{21}$$

where the Hill polarization tensor $\mathbb{P}_m$ is given by Withers' solution for ellipsoidal inclusions, in which elastic properties of the matrix m are used. In what follows, the undrained effective elastic tensor will be compared to macroscopic undrained properties experimentally obtained for a deep clay. The drained effective elastic tensor will be estimated and used to study Biot tensor. As an example, by using relations (6)–(20), in the particular case of an isotropic distribution of spherical inclusions in an isotropic matrix the effective Biot coefficient (relation 16) corresponding to Mori–Tanaka homogenization scheme can be written as (see Dormieux et al. (2006))

$$b^{\text{MT}}_{\text{sp}} = \frac{3f_p(1 - \nu_m)}{2(1 - 2\nu_m) + f_p(1 + \nu_m)} \tag{22}$$

$$\frac{1}{N^{\text{MT}}_{\text{sp}}} = \frac{3(1 - 2\nu_m)(1 + \nu_m)}{E_m} \frac{f_p(1 - f_p)}{2(1 - 2\nu_m) + f_p(1 + \nu_m)} \tag{23}$$

In this particular case, the effective Biot coefficient only depends on the porosity and the Poisson ratio of the matrix.

3.3. Effect of pore space geometry on poroelastic properties

At the opposite to man-made materials such as composites, the properties of all the constituents of geomaterials are not well known in common situation. Although experimental nano(poro)mechanics,

micro(poro)mechanics are actually a great field of research, in many situations only the *macroscopic*, or *effective*, mechanical or poromechanical properties have been characterized thanks to laboratory experiments such as geomechanical tests (as triaxial compression tests, and triaxial deviatoric tests) performed at the macroscopic scale. Even at the macroscopic scale, poromechanical coefficients, such as Biot tensor $\boldsymbol{B}$ and drained stiffness coefficients are very difficult to characterize in most low permeable geomaterials. The problem to solve may be seen as an inverse problem. As an example, the *homogenized* or *effective* properties and the pore space structure are more or less known and the unknown may be the matrix properties. The numerical results presented in this section are applied to the analysis of a transversely isotropic porous geomaterial: a deep clay (*Opalinus Clay*) from Mont Terri (Switzerland, approximately 200 meters depth) with porosity $f_p \approx 0.16$ (see Thury (2002)). Geomechanical laboratory tests such as undrained deviatoric triaxial compression tests allow to obtain the undrained elastic stiffness coefficients (see Giot (2004)): $E_1^{\text{undr}} = 22500$ MPa, $E_3^{\text{undr}} = 9000$ MPa, $\nu_{12}^{\text{undr}} = 0.14$, $\nu_{31}^{\text{undr}} = 0.15$, $G_{13}^{\text{undr}} = 2000$ MPa. By inverting relation (21) in which the data are the *effective* or *macroscopic* undrained elastic stiffness tensor $\mathbb{C}_{\text{undr}}^{\text{MT}}, f_p$ and $\mathbb{C}_p$ and the unknown is the elastic stiffness tensor of the argillaceous matrix $\mathbb{C}_m$, one obtains non-linear problem to solve

$$\mathbb{C}_m^{(i+1)} = \mathbb{C}_p + (\mathbb{C}_{\text{undr}}^{\text{MT}} - \mathbb{C}_p) : \left[\mathbb{I} + \frac{f_p}{(1-f_p)}[\mathbb{I} + \mathbb{P}_m^{(i)} : (\mathbb{C}_p - \mathbb{C}_m^{(i)})]^{-1}\right] \tag{24}$$

By iterative algorithm (24) is solved with initial condition

$$\mathbb{C}_m^{(0)} = \frac{\mathbb{C}_{\text{undr}}^{\text{MT}} - f_p\mathbb{C}_p}{1-f_p} \tag{25}$$

Three pore space geometries have been compared (O_{x_3} is the symmetry axis of the matrix and of the pore for cases 2 and 3)

- spherical pores (case 1),
- aligned flat ellipsoidal pores (aspect ratio $\varepsilon = b/a = 0.1$, case 2),
- aligned flat ellipsoidal pores (aspect ratio $\varepsilon = b/a = 0.03$, case 3),

After solving non-linear problem (24), the obtained matrix elastic tensor $\mathbb{C}_m$ is then used to estimate drained effective elastic tensor $\mathbb{C}_{\text{dr}}^{\text{MT}}$ (relation 20) and Biot tensor and solid Biot modulus thanks to relations (9, 10) with $\mathbb{C}^{\text{hom}} = \mathbb{C}_{\text{dr}}^{\text{MT}}$. Two parameters have been chosen to quantify the anisotropic degree of the transversely isotropic elastic tensor of the matrix $\mathbb{C}_m$. The first one denoted $A^{\text{hydrostatic}}$ and the second one denoted A^{uniaxial} are obtained by taking the ratio of two principal deformations respectively induced by an hydrostatic stress and uniaxial compression tests (in directions O_{x_1} and O_{x_3})

$$A^{\text{hydrostatic}} = \frac{1-2\nu_{31}^m}{(1-\nu_{12}^m)\frac{E_3^m}{E_1^m} - \nu_{31}^m}, \quad A^{\text{uniaxial}} = \frac{E_1^m}{E_3^m} \tag{26}$$

It may be noticed that a different parameter has been chosen by Withers (1989) on the basis of a cubic material (see Kelly and Macmillan (1986)). The parameter chosen by Withers is less adapted to transversely isotropic material than $A^{\text{hydrostatic}}$ and A^{uniaxial}. The two parameters $A^{\text{hydrostatic}}$ and A^{uniaxial} are equal to one in the isotropic case. Corresponding results are presented in Tables 2 and 3. As expected, with a given anisotropic degree of effective stiffness tensor, the (by definition isotropic) distribution of spherical pores, corresponds to the strongest anisotropic degree of the matrix. The influence of the pore shape on matrix

Table 1
Mineralogical composition, porosity and mechanical properties of Tournemire shale

Constituent	Volumetric fraction	Mechanical properties
Pore space	0.07	
Quartz (SiO_2)	0.20	Isotropic $E_{\text{qu}} = 96.4$ GPa, $\nu_{\text{qu}} = 0.08$
Calcite ($CaCO_3$)	0.15	Isotropic $E_{\text{ca}} = 84$ GPa, $\nu_{\text{ca}} = 0.3$
Argillaceous matrix	0.58	Transversely isotropic $E_1 = 22$ GPa, $E_3 = 7$ GPa, $G_{13} = 4$ GPa, $\nu_{12} = 0.12$, $\nu_{31} = 0.14$

Table 2
The parameters of the solid matrix m and the components of the Biot tensor

Case	E_1^m	E_3^m	ν_{12}^m	ν_{31}^m	G_{13}^m	b_1	b_3
1	32522.4	12025.3	0.0742	0.1366	2559.29	0.21224	0.21973
2	27804.2	19328.5	0.1401	0.1973	3454.16	0.23487	0.48856
3	27000.3	23800.1	0.1405	0.2529	8372.87	0.26788	0.59348

Table 3
Anisotropic degree

Case	A^{uniaxial}	$A^{\text{hydrostatic}}$
1	2.7045	3.53298
2	1.43851	1.51172
3	1.13446	0.979141

anisotropy can be analyzed by comparing cases 1 and 2. The corresponding Biot tensor values are very different. The distribution of spherical pores gives low values of Biot coefficients b_i for moderate porosity ($\phi \approx 0.15$–0.20), even if the solid matrix is transversely isotropic. A similar result can be noticed in the simplest case of isotropic matrix (see formula 23). In this material, the more realistic values are obtained with flat pores. The realistic pore shape is closer to very flat shape or *penny shape* than to spherical shape. For a given aspect ratio of the pores, the orientational distribution of the pores has a strong effect on the deviatoric part of the Biot tensor. The Biot tensor is closed to hydrostatic tensor in the case of an isotropic (or random) orientational distribution of flat oblate pores whereas its deviatoric part is not negligible with an aligned distribution of flat oblate pores. It may be noticed that no direct measurement of Biot coefficients have been performed on the Opalinus clay studied in this paper. This is due to the very low permeability of this material (intrinsic permeability of order 10^{-20}–10^{-21} m^2) the drained experiments necessary to measure Biot coefficients are extremely difficult to realize. In this context, the micromechanical approach is then useful to provide estimates of effective properties. By considering a transversely isotropic matrix elastic stiffness tensor $\mathbb{C}_m$ with moduli: $E_1^m = 27000.3$ MPa, $E_3^m = 23800.1$ MPa, $\nu_{12}^m = 0.1405$, $\nu_{31}^m = 0.2529$, $G_{13}^m = 8372.87$ MPa (it corresponds to the properties obtained in case 3, see Table 2), a sensitivity study is then performed on the aspect ratio of the pores $\varepsilon = b/a = 0.03, 0.1, 1$ to illustrate the effect of the pore geometry on effective poroelastic properties. Results are reported on Figs. 1–4 (drained case) for porosity comprised between 0 and 0.25). Respective anisotropic degree of drained and undrained effective elastic stiffness tensor (relations 20 and 21) are presented in Fig. 3. A strong decrease of the elastic modulus E_3 (direction perpendicular to the isotropic plane) with porosity is obtained for oriented flat oblate pores, $\varepsilon = b/a = 0.03, 0.1$, (see Fig. 1). At a given aspect ratio of the pores and for the same distribution of pores, the anisotropy degree of the undrained elastic tensor is much lower than that of the corresponding drained tensor (see Fig. 3). The difference between the two cases is a decreasing function of the aspect ratio. In the undrained case pores (in the saturated case) can be seen as elastic material with bulk modulus and zero shear coefficient. The inverse of the solid Biot modulus quantifies the coupling induced by pore pressure variations on porosity (see relation 10). As expected, the inverse of solid Biot modulus is an increasing function of the connected porosity (see Fig. 4). It is also interesting to compare the influence of pore shape at a given porosity: aligned flat pores with lower aspect ratio induce higher values of coefficient N^{-1} than spherical pores.

3.4. Application to porous argillaceous rocks with spherical inclusions

An application to a transversely isotropy shale containing spherical shape inclusions of mineral phases such as quartz and calcite is presented in this section. As in reference Ulm et al. (2005) a two-step homogenization scheme is performed:

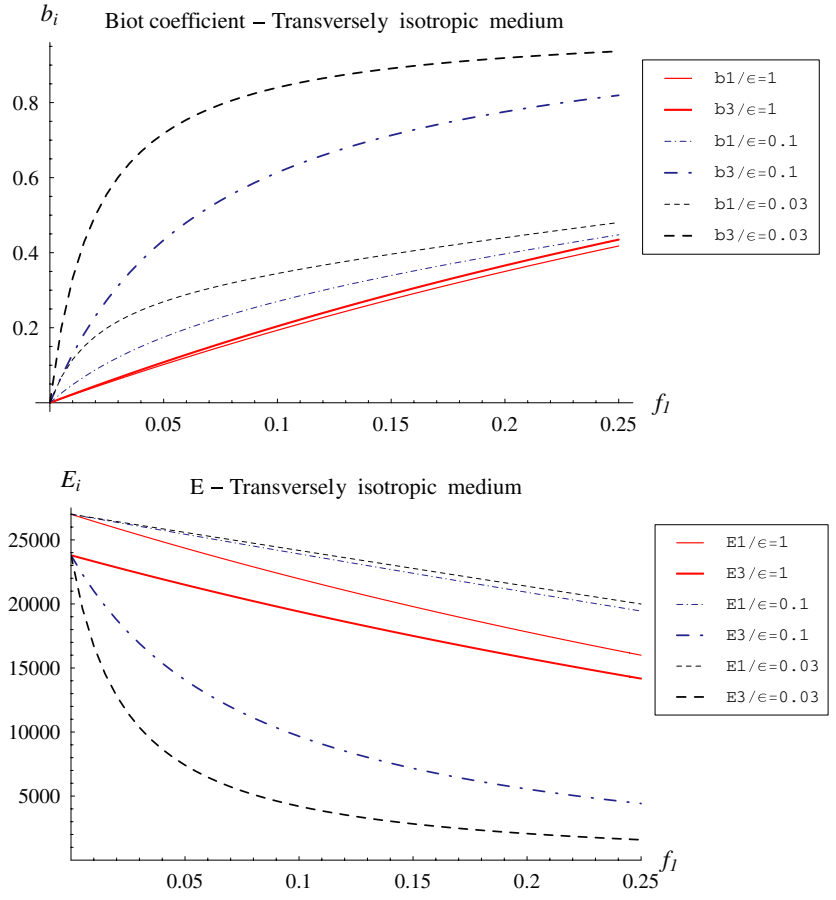

Fig. 1. Effective drained moduli E_i and Biot coefficients b_i.

1. The argillaceous matrix containing microporosity is first homogenized, the result is a transversely isotropic matrix denoted $\mathbb{C}^{\mathrm{I}}_{\mathrm{hom}}$, and Withers' solution (Withers (1989)) is used to approximate pore as flatted ellipsoidal inhomogeneities,
2. Spherical inclusions of mineral phases (such as quartz and calcite) are randomly added in the transversely isotropic porous argillaceous matrix obtained from the first step.

As in the previous section, the Mori–Tanaka homogenization scheme is used for the two steps. The first homogenization step can be performed by using relation (20) where the input are stiffness tensor of the clay matrix ($\mathbb{C}_m = \mathbb{C}^{\mathrm{clay}}$), porosity f_p, $\mathbb{P}$ tensor of aligned flat ellipsoidal pores of aspect ratio ε (Wither's solution), the output is the stiffness tensor $\mathbb{C}^{\mathrm{I}}_{\mathrm{hom}}$

$$\mathbb{C}^{\mathrm{I}}_{\mathrm{hom}} = (1-f_p)\mathbb{C}_m : [(1-f_p)\mathbb{I} + f_p[\mathbb{I} - \mathbb{P}_m : \mathbb{C}_m]^{-1}]^{-1} \tag{27}$$

$$\mathbb{C}_m = \mathbb{C}^{\mathrm{clay}}, \quad \mathbb{P}_m = \mathbb{P}_m(\varepsilon, \mathbb{C}_m) \tag{28}$$

In the general case of $r-1$ different mineral phase inclusions of spherical shape isotropically distributed, the second homogenization step performed by using Mori–Tanaka scheme reads

$$\mathbb{C}^{\mathrm{II}}_{\mathrm{hom}} = \mathbb{C}^{\mathrm{I}}_{\mathrm{hom}} + \left(\sum_{i=2}^{r} f_i(\mathbb{C}_i - \mathbb{C}^{\mathrm{I}}_{\mathrm{hom}}) : \mathbb{D}_i\right) : \left[\mathbb{I} + \sum_{i=2}^{r} f_i(\mathbb{D}_i - \mathbb{I})\right]^{-1} \tag{29}$$

$$\mathbb{D}_i = [\mathbb{I} + \mathbb{P}^{(i)}_m : (\mathbb{C}_i - \mathbb{C}^{\mathrm{I}}_{\mathrm{hom}})]^{-1}, \quad \mathbb{P}^{(i)}_m = \mathbb{P}(\mathbb{C}^{\mathrm{I}}_{\mathrm{hom}}) \tag{30}$$

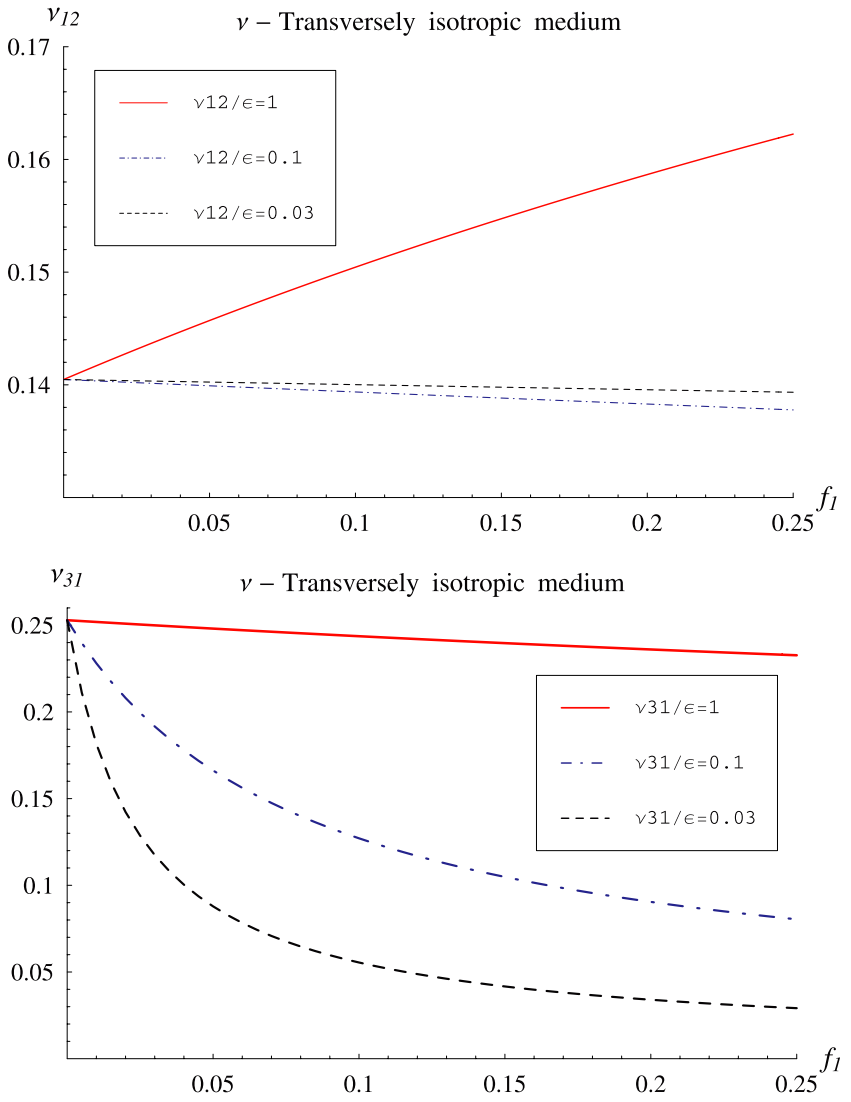

Fig. 2. Effective drained coefficients ν_{12} and ν_{31}.

The input of second homogenization step are the homogenized stiffness tensor obtained from the first homogenization step (argillaceous matrix and pores), denoted $\mathbb{C}^{\mathrm{I}}_{\mathrm{hom}}$, the volumetric fraction of each mineral phases f_i, and the elastic properties of each mineral phase (stiffness tensor $\mathbb{C}_i$). The studied material is a transversely isotropic shale from southern of France. Physical and mechanical properties of this material are described in references Valès et al. (2004), Charpentier et al. (2003) and Pietruszczak et al. (2002). They are presented in Table 1. Two mineral phases are considered, quartz and calcite which represent approximately 35% of the total volume of the material. The Mori–Tanaka homogenization scheme can be reasonably used in this case, even if the total volume fraction of inclusion is high, thanks to the spherical shape of inclusions and isotropic distribution. A sensitivity study has been performed on pore aspect ratio $0.03 \leqslant \varepsilon = b/a \leqslant 0.23$ and results are presented on Figs. 5–8. The two Biot coefficients b_1 and b_3 are decreasing functions of pore aspect ratio. It may be noticed that aspect ratio (approximately) higher than 0.2 are not realistic for this material and so the particular pore aspect ratio giving same components of Biot coefficient is not physically relevant. The respective anisotropic degree $A^{\mathrm{hydrostatic}}$ of the stiffness tensors $\mathbb{C}^{\mathrm{I}}_{\mathrm{hom}}$ (step 1, clay matrix and pores), $\mathbb{C}^{\mathrm{II}}_{\mathrm{hom}}$ homogenized stiffness tensor (step 2) are plotted in Figs. 7 and 8. As expected, the distribution of spherical inclusions of quartz

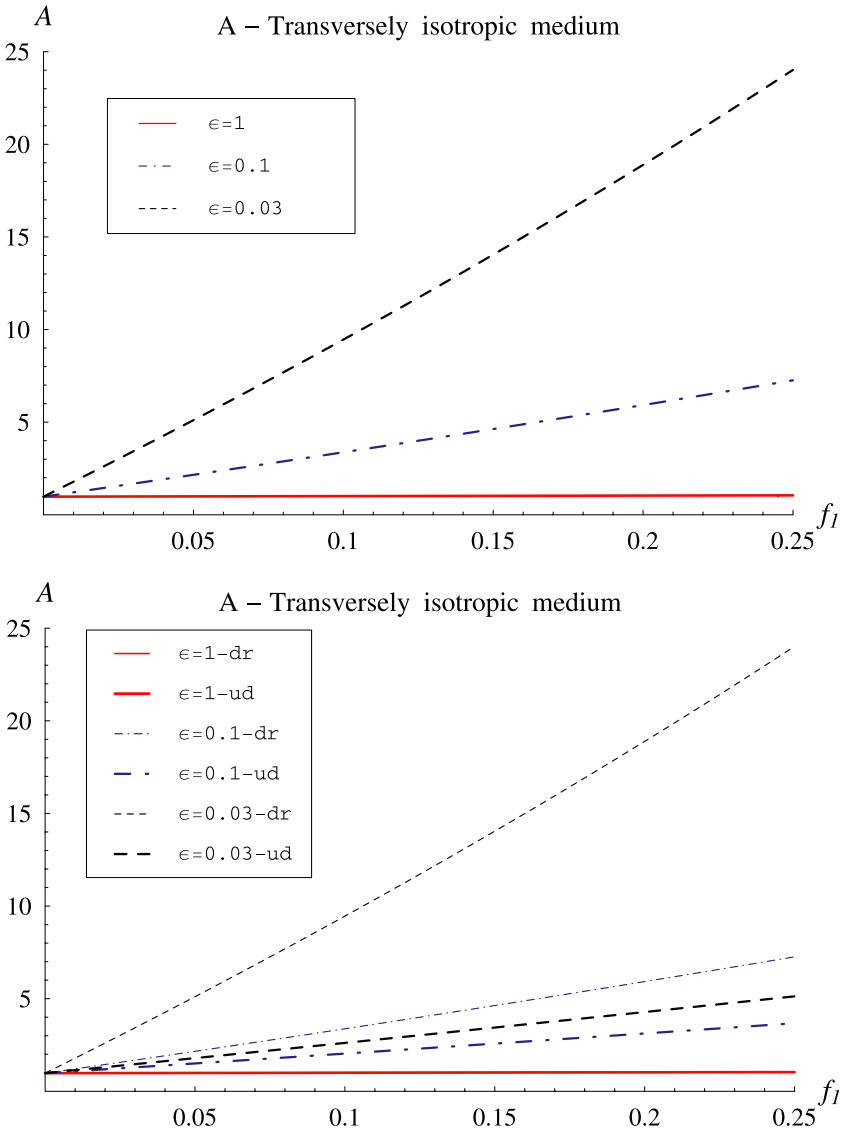

Fig. 3. Anisotropic degree.

and calcite (which are furthermore isotropic) strongly reduces the anisotropic degree of the material. Aligned distribution of flatted ellipsoidal pores would induce a very high anisotropic degree of the porous clay matrix stiffness tensor. The influence of pore aspect ratio on the solid Biot modulus is presented in Fig. 6. Again, it may be noticed that the inverse of Biot modulus is a decreasing function of the pore aspect ratio in the case of an aligned distribution of oblate pores in a transversely isotropic matrix. For this kind of material, more realistic estimate could be obtained by using Orientation Distribution Function (ODF) to represent pore distribution (see for instance Sayers (1994)).

4. Conclusions

The Withers' solution (Withers, 1989) for the problem of the ellipsoidal inclusion in a transversely isotropic solid matrix, has been applied to estimate effective poroelastic coefficients of rocks-like composites. The particular case of the spherical inclusion is useful for rock like composites which contains mineral solid inclusions

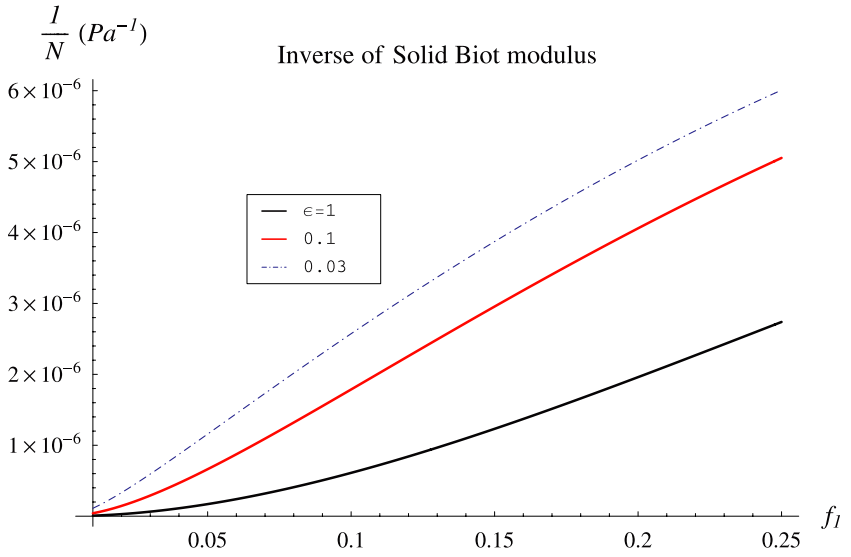

Fig. 4. Inverse of solid Biot modulus N.

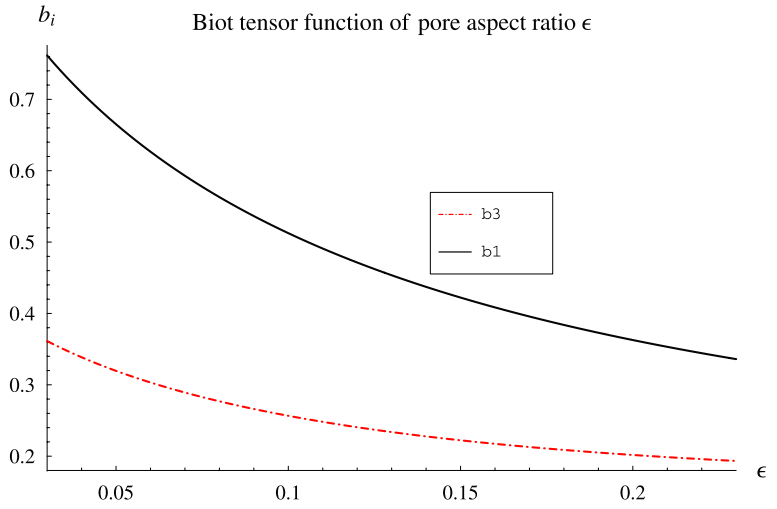

Fig. 5. Biot tensor function of pore aspect ratio ε.

with nearly spherical shapes. This class of anisotropic materials are studied in our laboratory and are current subject of research. In the case of the two particular shales, considered in the study, the spherical shape is more adapted to represent inclusions of solid mineral phases (such as quartz and carbonates) than pores which are, in most cases, better represented with flat ellipsoids. The effective transversely isotropic behaviour observed at the macroscopic scale is due to the pore space morphology (shape of pores, orientational distribution and spatial distribution) and to the anisotropy of the solid matrix itself. Compared to experimental results, more relevant results are obtained for oriented or randomly orientated distributions of flat pores. Further research would include the Orientation Distribution Function (ODF) to represent pore distribution. The assumption of anisotropic matrix is essential for multi-step homogenization methods. The homogenization schemes presented in this paper for rock-like composites such as shales will be generalized by including another steps to homogenized lower levels, starting from level of mineral aggregation (it corresponds to *nanoporomechanics*) or from level of clay mineral (level '0', see Ulm et al., 2005).

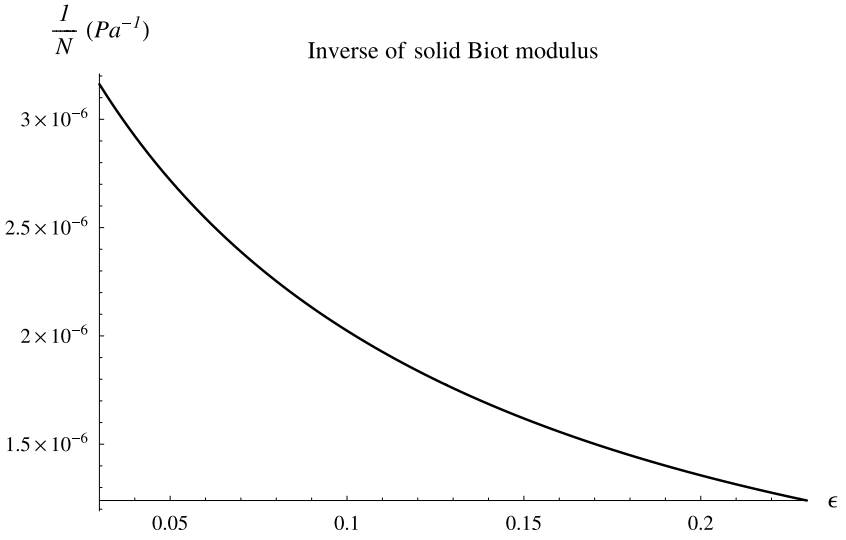

Fig. 6. Inverse of solid Biot modulus function of pore aspect ratio ε.

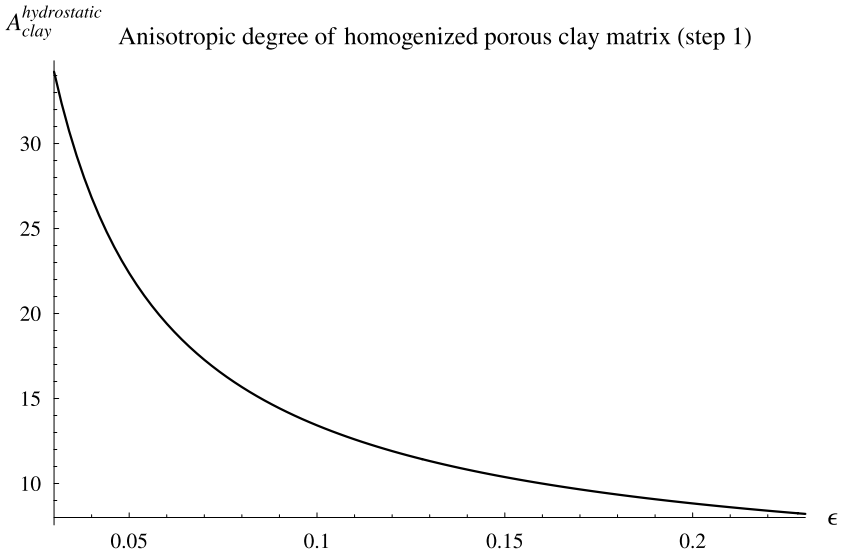

Fig. 7. Anisotropic degree of $\mathbb{C}_{\text{hom}}^{\text{I}}$ function of pore aspect ratio ε.

Appendix A. Elastic constants for transversely isotropic matrix

Matrix notations for elastic tensor $\mathbb{C}$ of a transversely isotropic material with axis of revolution Ox_3

$$\begin{aligned} &C_{1111} = C_{2222} = C_{11}, \quad C_{3333} = C_{33}, \quad C_{1212} = C_{66} \\ &C_{1122} = C_{2211} = C_{12}, \quad C_{1133} = C_{3311} = C_{2233} = C_{3322} = C_{13} \\ &C_{1313} = C_{2323} = C_{1331} = C_{2332} = C_{3113} = C_{3223} = C_{3131} = C_{3232} = C_{44} \end{aligned} \tag{31}$$

The compliance elastic tensor $\mathbb{S}$ and elastic tensor $\mathbb{C}$ of a transversely isotropic elastic solid with axis of revolution Ox_3 can be written as

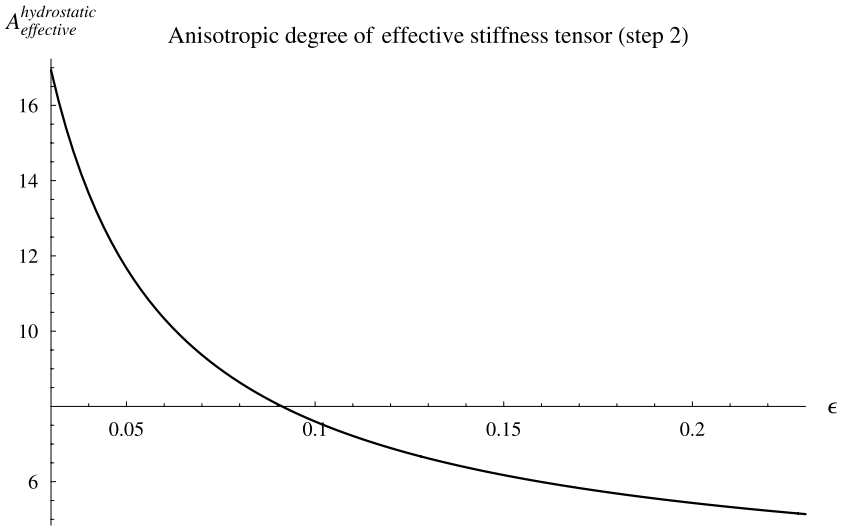

Fig. 8. Anisotropic degree of $\mathbb{C}^{\mathrm{II}}_{\mathrm{hom}}$ function of pore aspect ratio ε.

$$
\begin{aligned}
&S_{1111} = S_{2222} = \frac{1}{E_1}, \quad S_{3333} = \frac{1}{E_3}, \quad S_{1122} = -\frac{\nu_{12}}{E_1} \\
&S_{1133} = -\frac{\nu_{31}}{E_3}, \quad S_{1212} = \frac{1+\nu_{12}}{2E_1}, \quad S_{2323} = S_{3131} = \frac{1}{4G_{13}} \\
&C_{11} = -\frac{1-\nu_{31}^2\frac{E_1}{E_3}}{(1+\nu_{12})\left(\frac{2\nu_{31}^2}{E_3}-\frac{1-\nu_{12}}{E_1}\right)}, \quad C_{33} = \frac{E_3\left(\frac{1-\nu_{12}}{E_1}\right)}{\frac{2\nu_{31}^2}{E_3}-\frac{1-\nu_{12}}{E_1}} \\
&C_{12} = -\frac{\nu_{12}+\nu_{31}^2\frac{E_1}{E_3}}{(1+\nu_{12})\left(\frac{2\nu_{31}^2}{E_3}-\frac{1-\nu_{12}}{E_1}\right)}, \quad C_{13} = -\frac{\nu_{31}}{\frac{2\nu_{31}^2}{E_3}-\frac{1-\nu_{12}}{E_1}} \\
&C_{44} = G_{13}, \quad C_{66} = \frac{C_{11}-C_{12}}{2}
\end{aligned}
\tag{32}
$$

Relations (4) giving Eshelby tensor $\mathbb{S}^{\mathrm{E}}$ can be written as follows

$$
\begin{aligned}
&S^{\mathrm{E}\Omega}_{1111} = P_{11}C_{11} + P_{12}C_{12} + P_{13}C_{13}, \quad S^{\mathrm{E}\Omega}_{1122} = P_{11}C_{12} + P_{12}C_{11} + P_{13}C_{13} \\
&S^{\mathrm{E}\Omega}_{1133} = (P_{11}+P_{12})C_{13} + P_{13}C_{33}, \quad S^{\mathrm{E}\Omega}_{3311} = P_{13}(C_{11}+C_{12}) + P_{33}C_{13} \\
&S^{\mathrm{E}\Omega}_{3333} = 2P_{13}C_{13} + P_{33}C_{33}, \quad S^{\mathrm{E}\Omega}_{1313} = 2P_{44}C_{44}
\end{aligned}
$$

Appendix B. Hill polarization tensor for a spherical inclusion in a transversely isotropic medium

As in references Withers (1989), Mura (1987), the volume integral (3) can be expressed as a surface integral which can be written in terms of the solid angle $\mathrm{d}\omega$

$$
\mathrm{d}\Omega_{z'} = \mathrm{d}\Omega_{z'}(\underline{r}) = \mathrm{d}r\,\mathrm{d}S = r^2\mathrm{d}r\mathrm{d}\omega, \quad \underline{r} = \underline{z}' - \underline{z}, \quad r = |\underline{z}' - \underline{z}| \tag{33}
$$

Following the Withers' method, the derivatives of the Green's function G_{ij} are expressed thanks to g_{ijk} components

$$
g_{ijk}(\underline{\ell}) = r^2 G_{ij,k}(\underline{z}-\underline{z}') = -r^2 G_{ij,k}(\underline{r}), \quad \underline{\ell} = \frac{\underline{z}'-\underline{z}}{|\underline{z}'-\underline{z}|} = (\ell_1,\ell_2,\ell_3) \tag{34}
$$

By using (34) Eq. (3) becomes

$$\mathscr{M}^{\Omega}_{ijkl} = -\frac{\partial}{\partial z_l}\int_{\Sigma} r(\underline{\ell}) g_{ijk}(\underline{\ell}) \mathrm{d}\omega \tag{35}$$

Σdenotes the surface of an unit sphere centered at point $\underline{z}$ (Mura, 1987) and $r(\underline{\ell})$ defines the boundary of the sphere and is given by the positive root of the equation

$$\frac{(z_1 + r\ell_1)^2 + (z_2 + r\ell_2)^2 + (z_3 + r\ell_3)^2}{a^2} = 1 \tag{36}$$

where

$$r(\underline{\ell}) = -f + (f^2 + e)^{1/2}, \quad \begin{cases} e = a^2 - (z_1^2 + z_2^2 + z_3^2) \\ f = \ell_1 z_1 + \ell_2 z_2 + \ell_3 z_3 \end{cases} \tag{37}$$

Since g_{ijk} is odd in $\underline{\ell}$ while $(f^2 + e)^{1/2}$ is even in $\underline{\ell}$ it may be shown that

$$\mathscr{M}^{\Omega}_{ijkl} = \frac{\partial}{\partial z_l}\int_{\Sigma} f g_{ijk}(\underline{\ell}) \mathrm{d}\omega = \int_{\Sigma} \frac{\partial f}{\partial z_l} g_{ijk}(\underline{\ell}) \mathrm{d}\omega = \int_{\Sigma} \ell_l g_{ijk}(\underline{\ell}) \mathrm{d}\omega \tag{38}$$

and the components of $\mathbb{P}$ tensor read then

$$P^{\Omega}_{ijkl} = \frac{1}{4}\int_{\Sigma} (\ell_l g_{kij}(\underline{\ell}) + \ell_l g_{kji}(\underline{\ell}) + \ell_k g_{lij}(\underline{\ell}) + \ell_k g_{lji}(\underline{\ell})) \mathrm{d}\omega \tag{39}$$

The reader can find in the founding papers Eshelby (1957) (isotropic case) and Withers (1989) (transversely isotropic case) the method of analytical calculation of integrals 39 to obtain the components of Eshelby tensor in the general case of the ellipsoidal inclusion. Explicit expressions of Hill polarization components obtained by following the Withers' method in the particular case of the spherical inclusion are recalled in the next appendix.

B.1. Components of Hill polarization tensor

It may be noticed that the correction indicated by Pouya and Zaoui (2006) for a misprint in Pan and Chou (1976) has been taken into account in order to incorporate in the theory proposed by Withers (1989) the particular case ($C^*_{13} - C_{13} - 2C_{44} = 0$) which was not included. From practical point of view, this case corresponds to a class of matrix which includes isotropic materials. Elastic constants of isotropic (*material 1*) and transversely isotropic (*material 2*) media and corresponding components of Hill's tensor for a spherical inclusion are respectively given in Tables 4 and 5. It may be noticed that the results also numerically coincide with those obtained by Laws (1985) (by performing numerical integration of Fourier transform integrals).

Table 4
Elastic constants

Material	E_1	E_3	ν_{12}	ν_{31}	G_{13}
1	2	2	0.15	0.15	0.869565
2	2	10	0.25	0.25	1
	C_{11}	C_{33}	C_{12}	C_{13}	C_{44}
1	2.1118	2.1118	0.372671	0.372671	0.869565
2	2.1793	10.3448	0.57931	0.689655	1

Table 5
Hill's polarization tensor for spherical inclusion

Material	P_{11}	P_{33}	P_{12}	P_{13}	P_{44}
1	0.248039	0.248039	−0.045098	−0.045098	0.146569
2	0.238712	0.0674127	−0.0530286	−0.0175442	0.113153

$$C_{13}^{*}=(C_{11}C_{33})^{1/2},\quad k_i=\frac{C_{11}/v_i^2-C_{44}}{C_{13}+C_{44}},\quad D=\frac{1}{4\pi C_{44}v_3}$$
$$v_1=\left[\frac{(C_{13}^{*}-C_{13})(C_{13}^{*}+C_{13}+2C_{44})}{4C_{33}C_{44}}\right]^{1/2}+\left[\frac{(C_{13}^{*}+C_{13})(C_{13}^{*}-C_{13}-2C_{44})}{4C_{33}C_{44}}\right]^{1/2}$$
$$v_2=\left[\frac{(C_{13}^{*}-C_{13})(C_{13}^{*}+C_{13}+2C_{44})}{4C_{33}C_{44}}\right]^{1/2}-\left[\frac{(C_{13}^{*}+C_{13})(C_{13}^{*}-C_{13}-2C_{44})}{4C_{33}C_{44}}\right]^{1/2}$$
$$v_3=\left(\frac{C_{66}}{C_{44}}\right)^{1/2},\quad C_{66}=\frac{C_{11}-C_{12}}{2},\quad \rho^2=z_1^2+z_2^2,\quad R_i^2=\rho^2+v_i^2z_3^2$$

(a) If $C_{13}^{*}-C_{13}-2C_{44}\neq 0$

$$P_{11}=\frac{3}{2}\sum_{i=1}^{2}v_iA_i'I_1(i)+\frac{DI_1(3)}{4},\quad P_{12}=\frac{1}{2}\sum_{i=1}^{2}v_iA_i'I_1(i)-\frac{DI_1(3)}{4}$$
$$P_{13}=\sum_{i=1}^{2}k_iv_i^3A_i'I_2(i),\quad P_{33}=-2\sum_{i=1}^{2}k_i^2v_i^5A_i'I_2(i) \tag{40}$$
$$P_{44}=\frac{1}{4}\sum_{i=1}^{2}(1+k_i)v_i^3A_i'[I_2(i)-2k_iI_1(i)]+\frac{Dv_3^2I_2(3)}{8}$$

with

$$A_i=-B_i,\quad A_i'=B_i',\quad A_i=-2v_ik_iA_i'$$
$$v_1A_1=-v_2A_2=\frac{C_{13}+C_{44}}{4\pi(v_2^2-v_1^2)C_{33}C_{44}} \tag{41}$$
$$A_1'=-\frac{C_{44}-v_1^2C_{33}}{8\pi(v_2^2-v_1^2)v_1^2C_{33}C_{44}},\quad A_2'=-\frac{C_{44}-v_2^2C_{33}}{8\pi(v_2^2-v_1^2)v_2^2C_{33}C_{44}}$$

(b) If $C_{13}^{*}-C_{13}-2C_{44}=0$

$$P_{11}=3\left(\frac{C_{13}}{C_{13}+C_{44}}\right)B_1I_1(1)-6B_1I_{12}+\frac{D}{4}I_1(3)$$
$$P_{12}=\left(\frac{C_{13}}{C_{13}+C_{44}}\right)B_1I_1(1)-2B_1I_{12}-\frac{D}{4}I_1(3)$$
$$P_{13}=2B_1[-3I_1(1)+v_1^2I_2(1)+4I_{12}] \tag{42}$$
$$P_{33}=4v_1^2B_1\left[3I_1(1)-\left(\frac{C_{11}}{C_{13}+C_{44}}\right)I_2(1)-4I_{12}\right]$$
$$P_{44}=-B_1\left[3+v_1^2\left(3+\frac{C_{44}}{C_{13}+C_{44}}\right)\right]I_1(1)+\frac{B_1v_1^2}{2}\left(\frac{C_{13}}{C_{13}+C_{44}}\right)I_2(1)+4B_1(1+v_1^2)I_{12}+\frac{D}{8}v_3^2I_2(3)$$

with

$$v_1=v_2=(C_{11}/C_{33})^{1/4},\quad k_1=k_2=1,\quad R_1=R_2$$
$$B_1=B_2=-v_1\frac{C_{13}+C_{44}}{16\pi C_{11}C_{44}} \tag{43}$$
$$A_1'=A_2'=\frac{1}{16\pi C_{11}}=-B_1\frac{C_{44}}{v_1(C_{13}+C_{44})}$$
$$B_1'=B_2'=\frac{1}{16\pi C_{44}v_1^2}=-B_1\frac{C_{11}}{v_1^3(C_{13}+C_{44})}$$

B.2. I integrals for spherical inclusions

Only expressions of needed integrals, I_1, I_2 and I_{12} are recalled hereafter (see Withers (1989) for complete calculations of I_j integrals in the general case).

$$\underline{\ell} = (\sin\theta\cos\phi, \sin\theta\sin\phi, \cos\theta), \quad \hat{R}_i = (\sin^2\theta + v_i^2\cos^2\theta)^{1/2}, \tag{44}$$

$$I_1(i) = \int \frac{\ell_1^2}{\hat{R}_i^3}\mathrm{d}\omega = \int_{\phi=0}^{2\pi}\int_{\theta=0}^{\pi} \frac{\sin^3\theta\cos^2\phi \mathrm{d}\theta\,\mathrm{d}\phi}{\hat{R}_i^3} = 2\pi v_i \int_0^1 \frac{(1-x^2)\mathrm{d}x}{x^2(1-v_i^2)+v_i^2}$$

$$I_2(i) = \int \frac{\ell_3^2}{\hat{R}_i^3}\mathrm{d}\omega = \frac{4\pi}{v_i}\int_0^1 \frac{x^2}{x^2(1-v_i^2)+v_i^2}\mathrm{d}x \tag{45}$$

$$I_{12} = \int \frac{\ell_1^4}{\hat{R}_1^5}d\omega = \frac{3\pi v_1}{2}\int_0^1 \frac{(1-x^2)^2}{x^2(1-v_1^2)+v_1^2}\mathrm{d}x$$

If $v_i^2 < 1$,

$$I_1(i) = \frac{2\pi G}{v_i}(\arccos(v_i)(1+G^2) - G), \quad G = \frac{v_i}{\sqrt{1-v_i^2}} \tag{46}$$

$$I_2(i) = \frac{4\pi G^2}{v_i^3}(1 - G\arccos(v_i)) \tag{47}$$

If $v_i^2 > 1$,

$$I_1(i) = \frac{2\pi F}{v_i}(\operatorname{arccosh}(v_i)(1-F^2) + F), \quad F = \frac{v_i}{\sqrt{v_i^2-1}} \tag{48}$$

$$I_2(i) = \frac{4\pi F^2}{v_i^3}(F\ \operatorname{arccosh}(v_i) - 1) \tag{49}$$

If $v_i^2 = 1$,

$$I_1(i) = I_2(i) = \frac{4\pi}{3} \tag{50}$$

If $0 < v_1 < 1$,

$$I_{12} = \frac{3\pi G}{2v_1}\left[-\frac{5G}{3} - G^3 + (G^4 + 2G^2 + 1)\operatorname{arccot}(G)\right] \tag{51}$$

If $v_1 > 1$,

$$I_{12} = \frac{3\pi F}{2v_1}\left[\frac{5F}{3} - F^3 + (1-F^2)^2\operatorname{arccoth}(F)\right] \tag{52}$$

If $v_1 = 1$,

$$I_{12} = \frac{4\pi}{5} \tag{53}$$

References

Charpentier, D., Tessier, D., Cathelineau, M., 2003. Shale microstructure evolution due to tunnel excavation after 100 years and impact of tectonic paleo-fracturing. case of Tournemire, France. Engineering Geology 70 (1-2), 55–69.

Coussy, O., 2004. Poromechanics. Wiley, New York.

Coussy, O., Dormieux, L., Detournay, E., 1998. From mixture theory to biot's approach for porous media. International Journal of Solids and Structures 35, 4619–4635.

Dormieux, L., 2005. Linear poroelasticity. In: Applied Micromechanics of Porous Media, CISM, ed: L. Dormieux et F.J. Ulm.
Dormieux, L., Molinari, A., Kondo, D., 2002. Micromechanical approach to the behavior of poroelastic materials. Journal of the Mechanics and Physics of Solids 50 (10), 2203–2231.
Dormieux, L., Kondo, D., Ulm, F., 2006. Microporomechanics, first ed. Wiley, New York.
Dunn, M.L., Wienecke, H.A., 1997. Inclusions and inhomogeneities in transversely isotropic piezoelectric solids. International Journal of Solids and Structures 34 (27), 3571–3582.
Eshelby, J.D., 1957. The determination of the elastic field of an ellipsoidal inclusion, and related problems. Proceedings of the Royal Society Series A 241, 376–396.
Eshelby, J.D., 1961. Elastic inclusions and inhomogeneities. In: Sneddon, I.N., Hill, R. (Eds.), Progress in Solid Mechanics, vol. 2. North-Holland, Amsterdam, pp. 89–140.
Giot, R., Décembre 2004. Interprétation des mesures de contraintes par relaxation dans les formations argileuses profondes. Ph.D. thesis, INPL, Nancy.
Giraud, A., Huynh, Q.V., Hoxha, D., Homand, F., 2005. Tenseur de biot dans les argilites de l'est: résultats expérimentaux et analyse micromécanique. In: Microstructure et propriétés des matériaux. Presses de l'Ecole Nationale des Ponts et Chaussées, pp. 209–214.
Jakobsen, M., Johansen, T.A., 2005. The effects of drained and undrained loading on visco-elastic waves in rock-like composites. International Journal of Solids and Structures 42, 1597–1611.
Kelly, A., Macmillan, N.H., 1986. Strong Solids. Oxford University Press, England.
Kirilyuk, V.S., Levchuk, O.I., 2005. Stress state of a transversely isotropic medium with an arbitrarily oriented spheroidal inclusion. International Applied Mechanics 41 (2), 137–143.
Laws, N., 1985. A note on penny-shaped cracks in transversely isotropic materials. Mechanics of Materials 4, 209–212.
Levin, V.M., Markov, M.G., 2005. Elastic properties of inhomogeneous transversely isotropic rocks. International Journal of Solids and Structures 42, 393–408.
Lutz, M.P., Zimmerman, R.W., 2005. Effect of an inhomogeneous interphase zone on the bulk modulus and conductivity of a particulate composite. International Journal of Solids and Structures 42, 429–437.
Mikata, Y., 2000. Determination of piezoelectric Eshelby tensor in transversely isotropic piezoelectric solids. International Journal of Engineering Science 38 (6), 605–641.
Mikata, Y., 2001. Explicit determination of piezoelectric Eshelby tensors for a spheroidal inclusion. International Journal of Solids and Structures 38 (40–41), 7045–7063.
Mura, T., 1987. Micromechanics of defects in solids, 2nd ed. Martinus Nijhoff Publishers.
Nemat-Nasser, S., Hori, M., 1993. Micromechanics: overall properties of heterogenous materials. North Holland–Elsevier, Amsterdam.
Pan, Y.C., Chou, T.W., 1976. Point force solution for an infinite transversely isotropic solid. Journal of Applied Mechanics 43, 608–612.
Pietruszczak, S., Lydzba, D., Shao, J.F., 2002. Modelling of inherent anisotropy in sedimentary rocks. International Journal of Solids and Structures 39 (3), 637–648.
Ponte Castañeda, P., Willis, J.R., 1995. The effect of spatial distribution on the effective behavior of composite materials and cracked media. Journal of the Mechanics and Physics of Solids 43 (12), 1919–1951.
Pouya, A., Zaoui, A., 2006. A transformation of elastic boundary value problems with application to anisotropic behavior. International Journal of Solids and Structures 43 (16), 4937–4956.
Sayers, C.M., 1994. The elastic anisotropy of shales. Journal of Geophysical Research 99, 767–774.
Sevostianov, I., Yilmaz, N., Kushch, V., Levin, V., 2005. Effective elastic properties of matrix composites with transversely-isotropic phases. International Journal of Solids and Structures 42 (2), 455–476.
Suvorov, A.P., Dvorak, G.J., 2002. Rate form of the Eshelby and Hill tensors. International Journal of Solids and Structures 39, 5659–5678.
Thury, M., 2002. The characteristics of the Opalinus Clay investigated in the Mont Terri underground rock laboratory in Switzerland. Comptes Rendus Physique 3 (7–8), 923–933.
Torquato, S., 2002. Random Heterogenous MaterialsMicrostructure and Macroscopic Properties. Springer-Verlag, Berlin.
Ulm, F.J., Delafargue, A., Constantinides, G., 2005. Experimental microporomechanics. In: Dormieux, L., Ulm, J.F. (Eds.), Applied Micromechanics of Porous Materials. Springer, Berlin.
Valès, F., Nguyen, M.D., Gharbi, H., Rejeb, A., 2004. Experimental study of the influence of the degree of saturation on physical and mechanical properties in tournemire shale (france). Applied Clay Science 26 (1-4), 197–207.
Withers, P.J., 1989. The determination of the elastic field of an ellipsoidal inclusion in a transversely isotropic medium, and its relevance to composite materials. Philosophical Magazine A 59 (4), 759–781.
Xu, S., 1998. Modelling the effect of fluid communication on velocities in anisotropic porous rocks. International Journal of Solids and Structures 35 (34–35), 4685–4707.
Zaoui, A., 1997. Structural morphology and constitutive behaviour of microheterogeneous materials. In: Suquet, P. (Ed.), Continuum Micromechanics. Springer, New York, pp. 291–347.
Zheng, Q.S., Du, D.X., 2001. An explicit and universally applicable estimate for the effective properties of multiphase composites which accounts for inclusion distribution. Journal of the Mechanics and Physics of Solids 49, 2765–2788.